

CuO nanoclusters coated with mesoporous SiO₂ as highly active and stable catalysts for olefin epoxidation†Chaoqiu Chen,^{ab} Jin Qu,^{ab} Changyan Cao,^c Fang Niu^{ab} and Weiguo Song^{*a}

Received 29th December 2010, Accepted 22nd February 2011

DOI: 10.1039/c0jm04568c

A one-pot solvothermal synthetic method to prepare uniform CuO colloidal nanocrystal clusters (CNCs) with sizes of approximately 60 nm was developed. To enhance their stabilities, the CuO CNCs were coated with mesoporous SiO₂ shells to form CuO CNCs@meso-SiO₂ nanocomposites. The CuO CNCs as well as the CuO CNCs@meso-SiO₂ composite catalyst were characterized by transmission electron microscopy, small-angle X-ray diffraction and N₂ adsorption-desorption methods. These results indicate that the SiO₂ shells have winding mesoporous channels with an average size of 3.7 nm, which are very favorable for mass transfer and catalytic reactions. This nanocomposite catalyst exhibited excellent activity and stability in olefin epoxidation reactions. The structure of the composite catalyst remained intact after eight consecutive runs, while pure CuO CNCs severely aggregated after only 1 run.

Introduction

Morphology controlled transition metal oxide nanomaterials are promising materials in optical, electric and catalytic applications.^{1–4} In particular, cupric oxide (CuO) and cuprous oxide (Cu₂O) have shown exciting properties as catalysts, solid-state sensors and lithium-ion battery materials, owing to their low band-gap energy, high catalytic activity, non-toxic nature and abundant resources.^{5–13} Various CuO and Cu₂O nano/micro materials have been synthesized to explore their properties and application possibilities.

Compared to bulk particles, nano-sized particles are much more active and selective catalysts, due to their higher special surface areas and quantum-confinement effects.^{14–18} However, a major obstacle for practical use of the nanoparticles as catalysts is their tendency to aggregation under real reaction conditions. The nanoparticles are usually subject to sintering or coalescence to minimize their surface energies, thus losing their catalytic activity during practical applications.¹⁹ In order to suppress this

trend, some strategies including alloying and encapsulation have been developed. Encapsulating nanoparticles in thermally stable and chemically inert porous oxides shells can effectively prevent sintering of the nanoparticles by spatially separating the nanoparticles. In addition, the porous structure of the porous coating provides channels for the reaction species to reach the surface of the nanoparticles, thus allowing the catalytic reaction to occur. The effectiveness of this strategy has been demonstrated by several papers for supported and unsupported metal nanoparticle catalysts.^{20–27} However, these researches are focused on noble metal nanoparticles. There are few studies on designing aggregate-resistant systems with transition metal oxide nanomaterials with a 3-dimensional structure.

In this study, a fast one-pot solvothermal process to prepare uniform CuO colloidal nanocrystal clusters (CNCs) with a size of approximate 60 nm was developed. Structural characterization indicates that these CNCs consist of CuO nanocrystals. By prolonged reaction time, the CuO CNCs were converted to Cu₂O hollow nanospheres. Encapsulating the CuO CNCs into mesoporous SiO₂ shells resulted in CuO CNCs@meso-SiO₂ nanocomposites. The mesoporous SiO₂ shell offers a physical shield to prevent the aggregation of the CuO CNCs. As a result, this nanocomposite catalyst exhibited excellent activity and stability in olefin epoxidation reactions. The composite catalyst remained intact after eight runs. In sharp contrast, pure CuO CNCs lost their morphology after only one run.

Experimental**Materials**

Cupric acetate monohydrate ((CH₃COO)₂Cu·H₂O), hexadecyltrimethylammonium bromide (CTAB), urea ((NH₂)₂CO), ethanol (C₂H₆O), and commercial copper (II) oxide (CuO)

^aBeijing National Laboratory for Molecular Sciences (BNLMS), Institute of Chemistry, Chinese Academy of Sciences, Beijing, 100190, P. R. China. E-mail: wsong@iccas.ac.cn; Fax: (+86)10-62557908; Tel: (+86)10-62557908

^bGraduate School of Chinese Academy of Sciences, Beijing, 100049, P. R. China

^cSchool of Materials Science and Engineering, Harbin Institute of Technology, Harbin, 150001, P. R. China

† Electronic supplementary information (ESI) available: SEM images of commercially available CuO and the sample obtained at the same reaction conditions without the addition of surfactant PVP; TG profile of CuO CNCs; X-ray diffraction patterns of samples obtained at different reaction times; N₂ adsorption and desorption isotherms of CuO CNCs and Cu₂O hollow nanospheres; TEM image of CuO CNCs@meso-SiO₂ nanocomposite used for 720 h under strong stirring. See DOI: 10.1039/c0jm04568c

powder were all purchased from Sinopharm Chemical Reagent Co., Ltd. Polyvinylpyrrolidone (PVP) ($M_w = 55\ 000$) was purchased from Sigma-Aldrich. Norbornene, t-butylhydroperoxide (TBHP), cis-cyclooctene, styrene and trans-stilbene were all purchased from Alfa Aesar. All materials were directly used as received without further purification.

Preparation of CuO CNCs and hollow Cu₂O nanospheres

In a typical experiment, $(\text{CH}_3\text{COO})_2\text{Cu}\cdot\text{H}_2\text{O}$ (79 mg) and urea (48 mg) were added into 32 mL ethanol and stirred until totally dissolved, followed by the addition of PVP (145 mg) under ultrasonic conditions for a few minutes. Then the navy-blue solution was transferred into a 40 mL autoclave with a Teflon-liner and was heated to 180 °C for 1 or 12 h, for CuO CNCs and hollow Cu₂O nanospheres, respectively. Then the autoclave was cooled naturally. The products were collected by centrifugation, and washed with deionized water and ethanol several times. Finally the samples were dried at 40 °C in a vacuum oven overnight.

Preparation of CuO CNCs@meso-SiO₂ nanocomposite

The mesoporous silica shells coated CuO CNCs were prepared according to our previous method.²⁸ In a typical synthesis procedure, 24 mg of as-synthesized CuO CNCs were added to a solution of 30 mL H₂O, 20 mL ethanol and 0.124 g CTAB at room temperature. After sonication for 1 h, 60 μL of 1 M NaOH aqueous solution was added to the above solution under stirring. Then 0.12 mL of TEOS was added slowly drop-wise and maintained at room temperature for 12 h with vigorous stirring. The obtained samples were washed with deionized water and ethanol several times. The resulting products were subjected to a Soxhlet extraction with ethanol for 2 days to remove the CTAB.^{29,30} Finally the products were dried at 40 °C in a vacuum oven overnight.

Characterization

The size and morphology of the products were characterized by transmission electron microscopy (TEM, JEOL JEM-1011, operating at an accelerating voltage of 100 kV), scanning electron microscopy (SEM, JEOL-6701F) and high resolution TEM (HRTEM, JEM 2100F, operating at an accelerating voltage of 200 kV). X-ray diffraction (XRD) patterns were collected on a Rigaku D/max 2500 diffractometer with Cu K α radiation ($\lambda = 0.1542$ nm) at 40 kV and 100 mA. The small-angle XRD measurements were carried out in Rigaku D/max-2400 diffractometer equipped with a secondary graphite monochromator with Cu K α radiation ($\lambda = 0.154$ nm). Data were collected in a step-scan mode in the range of 0.6–6 degree with step-width of 0.02 and speed of 1 degree·min⁻¹. Fourier-transform IR (FTIR) spectra were recorded on a Bruker Tensor 27 instrument. The surface area of the products was measured by the Brunauer-Emmet-Teller (BET) method using N₂ adsorption and desorption isotherms on an Autosorb-1 analyzer. Pore size distribution plot was obtained by the Barrett-Joyner-Halenda (BJH) method. The weight content of the CuO in the CuO CNCs@meso-SiO₂ nanocomposite was obtained from inductively coupled plasma emission spectrometer (ICP-AES, Shimadzu) analysis.

Olefin epoxidation

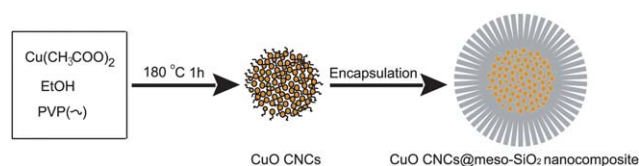
The epoxidation reactions were carried out in a 50 mL two-necked round bottom flask fitted with a reflux condenser. 10 mL of acetonitrile, 1 mmol alkene, 1 mmol diphenyl (as internal standard for GC analysis) and 10 mg CuO CNCs or CuO CNCs@meso-SiO₂ nanocomposite catalyst was mixed within the flask. Then 5 mmol TBHP was added drop-wise to the above mixture under vigorous stirring. The reaction was maintained at 70 °C for a desired time. The reaction mixture was sampled periodically for analysis by gas chromatography (Agilent 6890N GC) fitted with a HP-5 capillary column (30 m × 0.32 mm) and flame ionization detector, and a gas chromatography-mass spectroscopy (SHIMADZU, GCMS-QP2010S) method was applied for the identification product mixtures.

Results and discussion

Preparation of CuO CNCs and Cu₂O hollow nanospheres

Black CuO CNCs were synthesized *via* a one pot solvothermal reaction at 180 °C for 1 h, using $(\text{CH}_3\text{COO})_2\text{Cu}\cdot\text{H}_2\text{O}$ and urea as the starting materials, and ethanol as the solvent. PVP was employed as the surfactant to control the morphology of the product (Scheme 1). The morphology of the product was examined by TEM. As shown in Fig. 1a, the product is composed of a large quantity of well-dispersed colloidal clusters which include approximately 120 nanoparticles on average. The average diameter of these clusters was measured to be 60 ± 5 nm (Fig. 1a, 1b). The corresponding selected-area electron diffraction (SAED) shows typical ring patterns, indicating the polycrystalline nature of the CuO CNCs (Fig. 1c). HRTEM results show two different set of atomic lattice fringes in the same domain which correspond well with the $(\bar{1}11)$ and (111) crystallographic planes of the monoclinic CuO (Fig. 1d), further confirming the polycrystallinity of the CuO CNCs.

The XRD pattern of the CuO CNCs matches well those of crystalline CuO (Fig. 2a, JCPDS 65-2309). The average size of the CuO crystallites deduced from the Scherrer's equation for the strongest peak (111) is about 8 nm. The FT-IR spectrum (Fig. 2b) of the CuO nanostructure indicates two signature peaks at 524 cm⁻¹ and 586 cm⁻¹ from CuO.^{6,31} Three weak peaks at 2956 cm⁻¹, 1668 cm⁻¹, and 1426 cm⁻¹ were the characteristic peaks of PVP,³² indicating the presence of residual PVP on the CuO CNCs. Note that no calcination was carried out to prepare the samples. Based on TG data, the PVP is approximately 1.8 wt % in the sample (Fig. S1, ESI†). In a control experiment without the addition of PVP, CuO cubes and CuO spheres were obtained (Fig. S2, ESI†). These cubes and spheres have a wide size



Scheme 1 Overall synthetic scheme of CuO CNCs and the CuO CNCs@meso-SiO₂ nanocomposite.

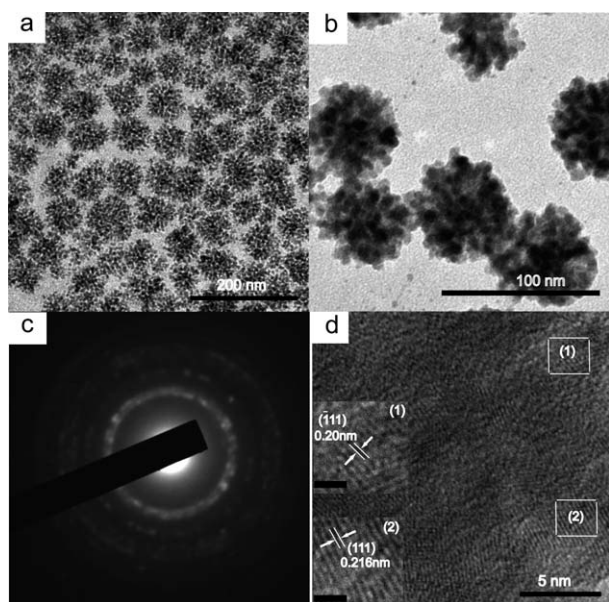


Fig. 1 TEM images of the as-prepared CuO CNCs: (a) low-magnification TEM image; (b) high-magnification TEM image and (c) the corresponding SAED pattern of an individual CuO CNCs; (d) HRTEM image taken from the individual CuO CNCs (insets: high-magnification HRTEM image of area marked with (1) and (2), respectively; scale bar = 1 nm).

distribution from 200 nm to 1 μm in size. These results suggested that the PVP helped to control the size of the nanocrystal clusters and the formation of the spherical geometry. The as-synthesized CuO CNC sample has a relatively high specific surface area of $80 \text{ m}^2 \cdot \text{g}^{-1}$, which is favorable for the catalytic performance (Fig. S3, ESI †).

Interestingly, when the reaction time was increased to 12 h, Cu_2O hollow nanospheres with a diameter of $110 \pm 15 \text{ nm}$ were produced (Fig. 3e). The HRTEM image shows the polycrystalline nature of these hollow nanospheres (Fig. 3f). As shown in Fig. 2a, the XRD pattern of the hollow nanospheres can be indexed to the cubic phase of Cu_2O (JCPDS 65-3288). No reflections of CuO were observed, confirming a complete transformation from CuO to Cu_2O . The FT-IR spectrum of the hollow nanospheres (Fig. 2b) shows that the characteristic peaks of CuO have disappeared. The new absorption band at 630 cm^{-1} can be assigned to Cu_2O .³³ The specific surface area of the hollow nanospheres is $62 \text{ m}^2 \cdot \text{g}^{-1}$ (Fig. S3, ESI †).

To investigate the mechanism of the transformation from CuO CNCs to Cu_2O hollow nanospheres, products were sampled at different reaction times and characterized by TEM (Fig. 3) and XRD. As shown in Fig. 3b, solid nanospheres are obtained after 2 h at 180°C . After 4 h of reaction (Fig. 3c), small voids can be seen in the center. With an increased reaction time, the voids in the center became bigger. After 12 h, the conversion is completed, leading to hollow nanospheres with well-centered circular voids (Fig. 3e). XRD patterns show that the peaks from CuO weakened sharply and new peaks from Cu_2O appeared after 2 h (Fig. S4, ESI †). The exact conversion mechanism from CuO to Cu_2O will be the subject of another study. This work mainly focused on the catalytic ability of CuO CNCs.

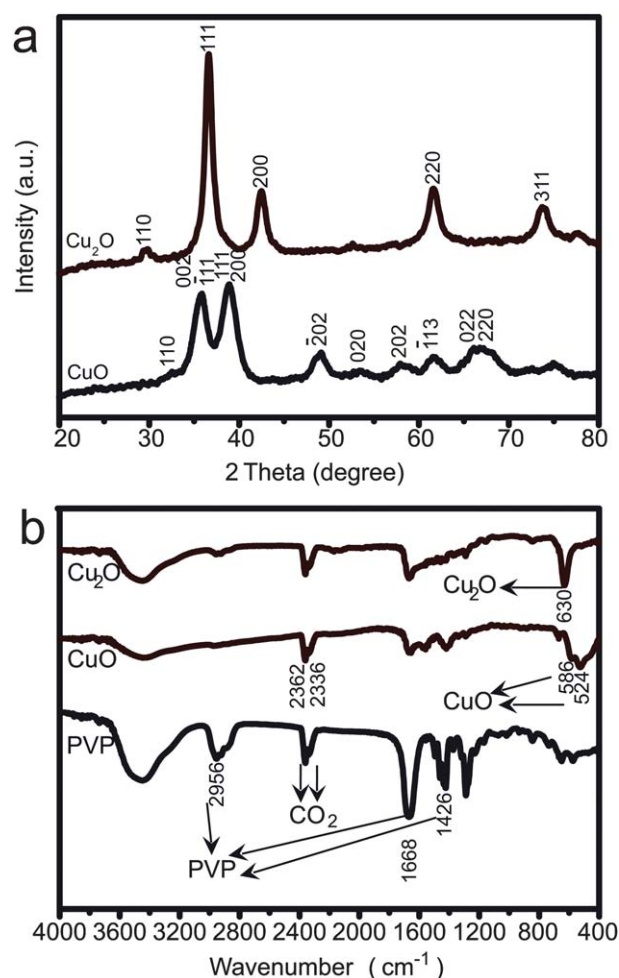


Fig. 2 (a) X-ray diffraction patterns of as-prepared CuO CNCs and Cu_2O hollow spheres and (b) FT-IR spectra of PVP, as-prepared CuO CNCs and as-prepared Cu_2O hollow spheres.

Preparation of CuO CNCs@meso- SiO_2 nanocomposite

For better mass transportation of the reaction species, porous shells are usually preferred.³⁴ In previous works, we developed a method to produce silica nanotubes with mesoporous walls and various internal morphologies. The hierarchical pore structure shows faster mass transportation in catalysis.²⁸ In this study, we used a similar strategy to encapsulate CuO CNCs in mesoporous SiO_2 shells. As shown in Fig. 4a and 4b, the TEM images show that CuO CNCs were evenly coated with a layer of mesoporous shells about 40 nm thick, while the CuO CNCs remained in their initial cluster morphologies (Fig. 1a). The inset of Fig. 4b shows the HRTEM image of the CuO CNCs core in the CuO CNCs@meso- SiO_2 nanocomposite. Small-angle XRD and N_2 adsorption-desorption analysis data are shown in Fig. 5. The small-angle XRD pattern of a CuO CNCs@meso- SiO_2 nanocomposite has a broad peak at around 2.5° (Fig. 5a), indicating that the mesoporous SiO_2 shells have relatively ordered mesopores. This is consistent with TEM results (Fig. 4b) and similar mesoporous materials.²⁸ The CuO CNCs@meso- SiO_2 nanocomposite exhibits a type IV adsorption isotherm with a narrow hysteresis loop (Fig. 5b). The surface area of the nanocomposite

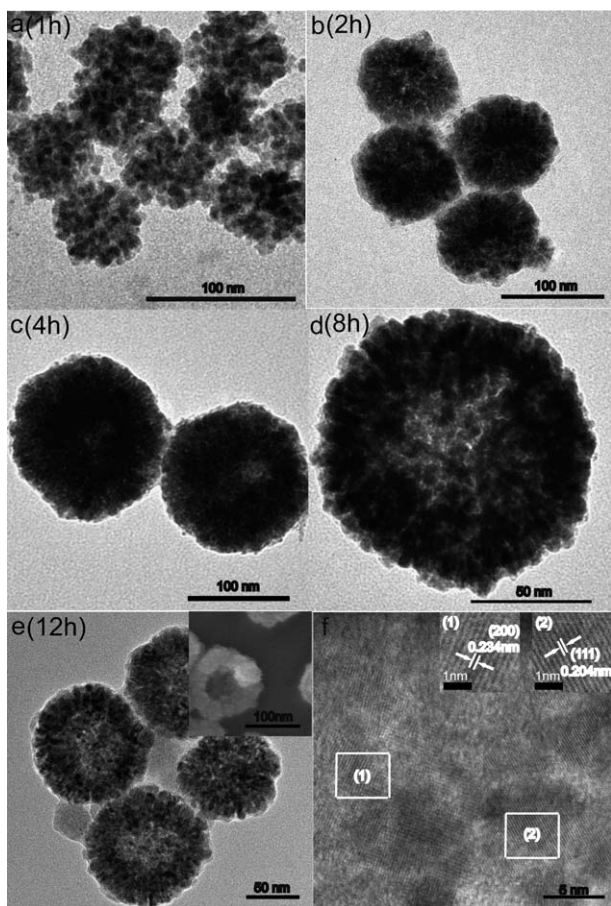


Fig. 3 TEM characterization of the samples obtained with different reaction times (a) 1 h, (b) 2 h, (c) 4 h, (d) 8 h, and (e) 12 h (inset: SEM image of a broken Cu_2O hollow sphere); (f) HRTEM image taken from the Cu_2O hollow sphere (insets: high-magnification HRTEM image of area marked with (1) and (2), respectively).

is $860.6 \text{ m}^2 \cdot \text{g}^{-1}$. The inset of Fig. 5b shows the BJH pore size distribution with a sharp peak at 3.7 nm, which was likely due to the average diameter of the pores in the mesoporous SiO_2 shells. All these results suggested that the silica coating on the composite is mesoporous silica, which provide efficient channels for mass transfer and catalytic reactions. The weight content of the CuO in the $\text{CuO CNCs@meso-SiO}_2$ nanocomposite was 27.2% according to ICP analysis results.

Catalytic performance in olefin epoxidation

The CuO CNCs , $\text{CuO CNCs@meso-SiO}_2$ nanocomposite and Cu_2O hollow nanospheres were used as catalysts for norbornene epoxidation using *t*-butylhydroperoxide (TBHP) as the oxidant and acetonitrile as the solvent. For comparison, commercial available CuO powder (SEM image is shown in Fig. S5, ESI[†]) was also tested. The norbornene conversion as a function of reaction time is shown in Fig. 6a. Both CuO CNCs and $\text{CuO CNCs@meso-SiO}_2$ nanocomposite had decent initial activities, resulting in 68% and 71% yield of norbornene epoxide in 1 h, respectively, and 100% selectivity for the epoxidation product;

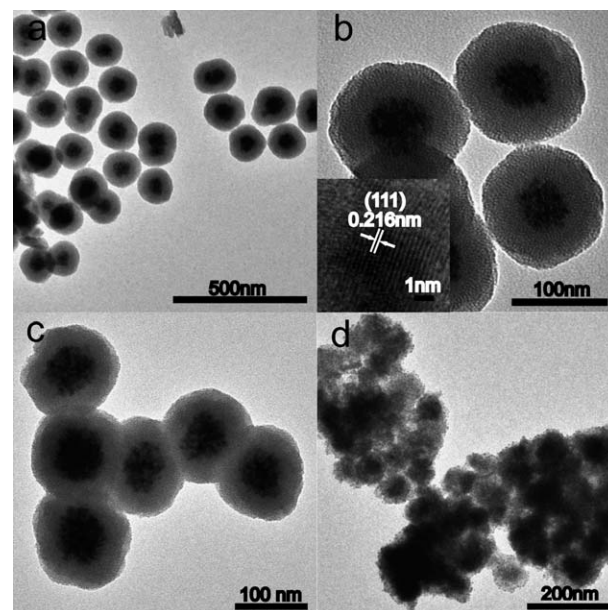


Fig. 4 (a) Low-magnification TEM image of the $\text{CuO CNCs@meso-SiO}_2$ nanocomposite; (b) high-magnification TEM image of the $\text{CuO CNCs@meso-SiO}_2$ nanocomposite (inset: HRTEM image taken from the CuO CNCs core in the $\text{CuO CNCs@meso-SiO}_2$ nanocomposite); (c) TEM image of the $\text{CuO CNCs@meso-SiO}_2$ nanocomposite after eight runs of olefin epoxidation; (d) TEM image of CuO CNCs used for 4 h of olefin epoxidation.

whereas the commercial CuO only resulted in a 20% yield after 1 h.

Besides TBHP, other cheaper oxidants such as H_2O_2 , O_2 and air were also tested for norbornene epoxidation, but unfortunately these oxidants didn't work under these reaction conditions.

Based on the catalytic results within 1 h of reaction in Fig. 6a, the turnover frequency (TOF) of norbornene epoxide formation in $\text{CuO CNCs@meso-SiO}_2$ nanocomposite and commercial CuO were $5.77 \times 10^{-3} \text{ s}^{-1}$ and $0.44 \times 10^{-3} \text{ s}^{-1}$, respectively, indicating that $\text{CuO CNCs@meso-SiO}_2$ nanocomposite is apparently much more active than commercial CuO powder. However, the surface area of CuO CNCs is $80 \text{ m}^2/\text{g}$, and the surface area of commercial

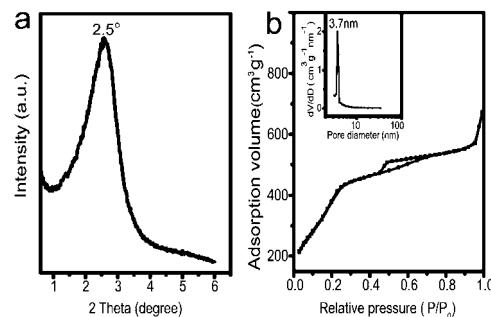


Fig. 5 (a) Small-angle XRD pattern of the $\text{CuO CNCs@meso-SiO}_2$ nanocomposite; (b) N_2 adsorption-desorption isotherms of the $\text{CuO CNCs@meso-SiO}_2$ nanocomposite (inset: the BJH pore diameter distribution curve at desorption branch).

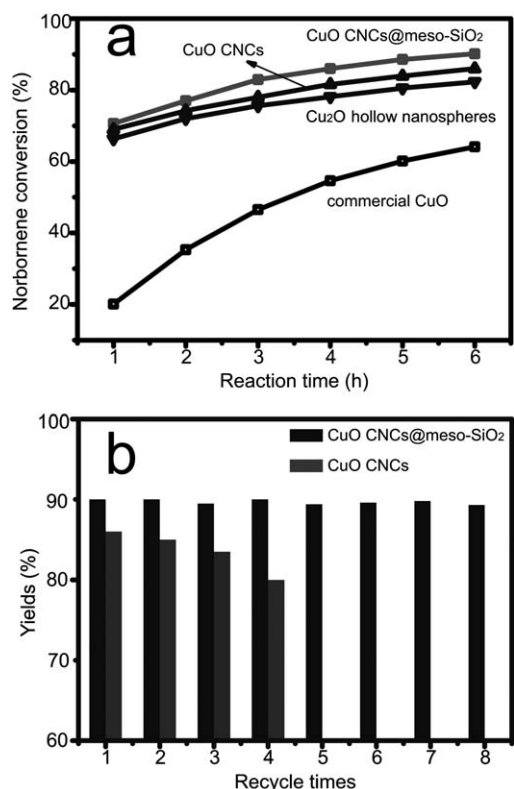


Fig. 6 (a) Norbornene conversion as a function of the reaction time over the CuO CNCs@meso-SiO₂ nanocomposite, CuO CNCs, Cu₂O hollow nanospheres and commercial CuO. Conditions: 1 mmol norbornene, 5 mmol TBHP, 10 mg catalyst, stirred in 10 mL of acetonitrile under reflux (70 °C). (b) Recycling results for epoxidation of norbornene, conditions: 1 mmol norbornene, 5 mmol TBHP, 10 mg catalyst, stirred in 10 mL of acetonitrile under reflux (70 °C) for 6 h.

CuO is 1.2 m²/g. Thus we also compared the TOF per surface Cu atom (by calculating the TOF per unit of surface area, as the number of surface Cu atoms is proportional to the surface area of the CuO), we found that the per surface area based TOF ratio between CuO CNCs@meso-SiO₂ nanocomposite and commercial CuO is about 1 : 5, indicating that the active sites on commercial CuO were actually more active than those on CuO CNCs. The apparently higher activity of CuO CNCs catalyst was due to its much higher surface area and much more active sites than commercial CuO.

The Cu₂O hollow nanospheres also can catalyze the epoxidation, giving a 66.3% conversion and 100% selectivity for norbornene epoxide within 1 h. XRD patterns of the used catalysts (Fig. S6, ESI†) show that the oxidation states of Cu in the catalysts remain after the reaction, indicating that all CuO and Cu₂O can catalyze the epoxidation.

Epoxidation reactions of cis-cyclooctene, styrene and trans-stilbene were also carried out and the results are summarized in Table 1. After refluxing in acetonitrile for 8 h, cis-cyclooctene gave a 66.5% conversion and 100% selectivity to the corresponding epoxide. However, other olefins, such as styrene and trans-stilbene have lower epoxide selectivities.

Catalytic epoxidations of styrene and trans-stilbene as a function of the reaction time and reaction temperature were carried out to compare the selectivities of these two reactions at different conversions. We found interesting patterns of selectivity changes at different reaction times as shown in Fig. S7, S8 and Table S1, ESI†. At lower alkene conversion (at the beginning of the reaction, or with lower reaction temperature, the selectivities were actually much lower, *i.e.* the undesired side reaction dominated). However, with higher alkene conversions (70 °C), the alkene epoxide selectivities were enhanced with increased reaction time. We propose that the side reactions (oxidative cleavage of alkene¹⁰) were faster than the epoxidation reactions, but the active sites for these side reactions were deactivated quickly, thus the epoxide products' selectivities were enhanced with longer reaction times. At higher reaction temperature, the alkene conversions increased but the selectivities of epoxides decreased, probably due to "over reaction".

More importantly, the CuO CNCs@meso-SiO₂ nanocomposite showed remarkable stability. The cycling performance of the CuO CNCs and CuO CNCs@meso-SiO₂ nanocomposite are shown in Fig. 6b, the CuO CNCs@meso-SiO₂ nanocomposite had no obvious loss of activity for eight consecutive runs; the norbornene epoxide yields were around 90% in all eight runs. In contrast, the norbornene epoxide yields decreased steadily in four runs using CuO CNCs as catalyst.

The TEM image of CuO CNCs sampled after refluxing for 4 h (Fig. 4d) shows that the CuO CNCs severely aggregated during the reaction process, resulting in a lower yield for norbornene epoxidation in the following runs. However, the TEM image of the CuO CNCs@meso-SiO₂ nanocomposite remained unchanged after 8 runs (Fig. 4c). In an extended stability test, the CuO CNCs@meso-SiO₂ nanocomposite was continuously stirred in the same reaction mixture for 720 h, most of the nanocomposites still maintained their morphologies (Fig. S9, ESI†). These results demonstrate that the mesoporous SiO₂ shell could serve as an effective protection against the destruction of CuO CNCs.

Conclusions

In summary, we prepared uniform CuO CNCs *via* a fast one-pot solvothermal synthetic route. CuO CNCs were coated with mesoporous SiO₂ shells to build an aggregate-resistant catalyst system. The CuO CNCs@meso-SiO₂ nanocomposite exhibited excellent catalytic activity and stability for olefin epoxidation reactions. The nanocomposite remained intact after eight runs. This strategy can be extended to design other catalytic systems with different shapes and compositions.

Acknowledgements

We thank the financial support from the National Natural Science Foundation of China (NSFC 50725207, 20821003), Ministry of Science and Technology (MOST 2007CB936400, 2009CB930400) and the Chinese Academy of Sciences (KJCX2-YW-N40).

Table 1 Epoxidation of Alkenes with CuO^a

Catalyst	Substrate	Product	Time, h	Conversion, %	Selectivity, %
CuO CNCs@meso-SiO ₂ nanocomposite			6	90	100
CuO CNCs			6	86	100
Cu ₂ O hollow nanospheres			6	82.3	100
Commercial CuO			6	64.2	100
CuO CNCs@meso-SiO ₂ nanocomposite			8	66.5	100
CuO CNCs@meso-SiO ₂ nanocomposite			2	88.6	61.2
CuO CNCs@meso-SiO ₂ nanocomposite			4	87.7	80.9

^a 1 mmol alkene, 5 mmol TBHP, and 10 mg catalyst, stirred in 10 mL of acetonitrile under reflux (70 °C).

Notes and references

- J. C. Park, J. Kim, H. Kwon and H. Song, *Adv. Mater.*, 2009, **21**, 803–807.
- P. Li, C. Nan, Z. Wei, J. Lu, Q. Peng and Y. Li, *Chem. Mater.*, 2010, **22**, 4232–4236.
- Y. Xia, P. Yang, Y. Sun, Y. Wu, B. Mayers, B. Gates, Y. Yin, F. Kim and H. Yan, *Adv. Mater.*, 2003, **15**, 353–389.
- Y. Sun and Y. Xia, *Science*, 2002, **298**, 2176–2179.
- F. Niu, Y. Jiang and W. Song, *Nano Res.*, 2010, **3**, 757–763.
- M. Basu, A. K. Sinha, M. Pradhan, S. Sarkar, A. Pal and T. Pal, *Chem. Commun.*, 46, pp. 8785–8787.
- L.-I. Hung, C.-K. Tsung, W. Huang and P. Yang, *Adv. Mater.*, 2010, **22**, 1910–1914.
- H. Zhang, Q. Zhu, Y. Zhang, Y. Wang, L. Zhao and B. Yu, *Adv. Funct. Mater.*, 2007, **17**, 2766–2771.
- J. Gao, Q. Li, H. Zhao, L. Li, C. Liu, Q. Gong and L. Qi, *Chem. Mater.*, 2008, **20**, 6263–6269.
- L. Xu, S. Sithambaram, Y. Zhang, C.-H. Chen, L. Jin, R. Joesten and S. L. Suib, *Chem. Mater.*, 2009, **21**, 1253–1259.
- J. Zhang, J. Liu, Q. Peng, X. Wang and Y. Li, *Chem. Mater.*, 2006, **18**, 867–871.
- Y. Cao, J. Fan, L. Bai, F. Yuan and Y. Chen, *Cryst. Growth Des.*, 2009, **10**, 232–236.
- H. Zhu, J. Wang and G. Xu, *Cryst. Growth Des.*, 2008, **9**, 633–638.
- I. Lee, F. Delbecq, R. Morales, M. A. Albitar and F. Zaera, *Nat. Mater.*, 2009, **8**, 132–138.
- E. Roduner, *Chem. Soc. Rev.*, 2006, **35**, 583–592.
- D. Wang, T. Xie and Y. Li, *Nano Res.*, 2009, **2**, 30–46.
- G. A. Somorjai, H. Frei and J. Y. Park, *J. Am. Chem. Soc.*, 2009, **131**, 16589–16605.
- G. A. Somorjai and J. Y. Park, *Angew. Chem., Int. Ed.*, 2008, **47**, 9212–9228.
- A. Cao, R. Lu and G. Veser, *Phys. Chem. Chem. Phys.*, 12, pp. 13499–13510.
- Z. Chen, Z.-M. Cui, F. Niu, L. Jiang and W.-G. Song, *Chem. Commun.*, 2010, **46**, 6524–6526.
- Y. Dai, B. Lim, Y. Yang, C. M. Cobley, W. Li, E. C. Cho, B. Grayson, P. T. Fanson, C. T. Campbell, Y. Sun and Y. Xia, *Angew. Chem., Int. Ed.*, 2010, **49**, 8165–8168.
- S. Kim, Y. Yin, A. P. Alivisatos, G. A. Somorjai and J. T. Yates, *J. Am. Chem. Soc.*, 2007, **129**, 9510–9513.
- H.-P. Zhou, H.-S. Wu, J. Shen, A.-X. Yin, L.-D. Sun and C.-H. Yan, *J. Am. Chem. Soc.*, 132, pp. 4998–4999.
- K. Yu, Z. Wu, Q. Zhao, B. Li and Y. Xie, *J. Phys. Chem. C*, 2008, **112**, 2244–2247.
- P. M. Arnal, M. Comotti and F. Schüth, *Angew. Chem., Int. Ed.*, 2006, **45**, 8224–8227.
- Q. Zhang, T. Zhang, J. Ge and Y. Yin, *Nano Lett.*, 2008, **8**, 2867–2871.
- K.-T. Li, M.-H. Hsu and I. Wang, *Catal. Commun.*, 2008, **9**, 2257–2260.
- S.-W. Bian, Z. Ma, L.-S. Zhang, F. Niu and W.-G. Song, *Chem. Commun.*, 2009, 1261–1263.
- G. Fanta and W. Doane, US Patents, 1986, 4605640.
- Y. Guo, A. Mylonakis, Z. Zhang, G. Yang, P. I. Lekes, S. Che, Q. Lu and Y. Wei, *Chem.-Eur. J.*, 2008, **14**, 2909–2917.
- Y. Liu, Y. Chu, M. Li, L. Li and L. Dong, *J. Mater. Chem.*, 2006, **16**, 192–198.
- Z. Hou, R. Chai, M. Zhang, C. Zhang, P. Chong, Z. Xu, G. Li and J. Lin, *Langmuir*, 2009, **25**, 12340–12348.
- R. V. Kumar, Y. Mastai, Y. Diamant and A. Gedanken, *J. Mater. Chem.*, 2001, **11**, 1209–1213.
- V. Suryanarayanan, A. S. Nair, R. T. Tom and T. Pradeep, *J. Mater. Chem.*, 2004, **14**, 2661–2666.